Extraordinary Optical Transmission Through Periodic Structures in Gold

Radboud Pos

July 20, 2012

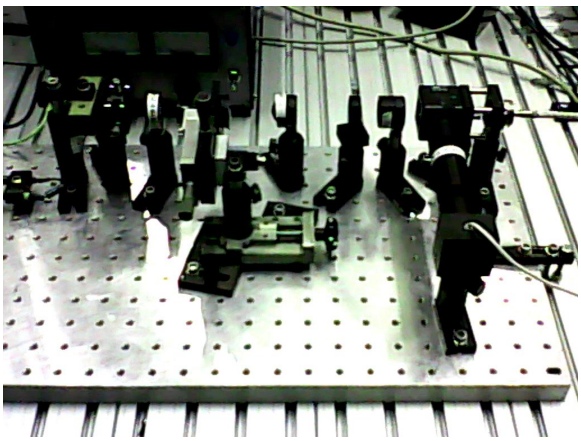

Universiteit Utrecht

Atom Optics and Ultrafast Dynamics
Utrecht University
Supervisors:
Dr. D. van Oosten
B.O. Mußmann

Abstract

In this thesis, the results of a research project on Extraordinary Optical Transmission (EOT) through a gold film containing periodic hole structures are reported. The *Poor Man's Setup* built for this research consisted of a white light LED for illumination purposes and an OceanOptics S2000 spectrometer for measuring spectra. The setup proved capable of reproducibly measuring EOT and allowing quantitative analysis of the spectrum. The measured enhanced transmission peaks occured at wavelengths ranging from where theory predicted transmission peaks to occur up to positions 4% red-shifted with respect to theoretical calculations. The RAYLEIGH anomaly was observed at the predicted wavelength of 770 nm, equalling the periodicity of the structures.

The structures on which measurements were done consisted of a 90 nm thick gold film on a glass substrate with a periodic array having a pitch of 770 nm. The apertures in the structures consisted of square holes ranging in width from 160 nm to 590 nm.

Contents

Chapter 1

Introduction

1.1 Outline

In this thesis the research and corresponding results of using a *Poor Man's Setup* for measuring Extraordinary Optical Transmission (EOT) of ten well-defined periodic structures are presented.
Chapter 1 will treat, apart from this overview, a general introduction on the discovery of EOT and give the prime motivation for doing research on EOT, including the motivation for doing this research.
In the second chapter the underlying theory necessary to understand EOT will be treated. After a general treatment of aperture theory for small apertures and treatment of the characteristics of Surface Plasmon Polaritons, it will be shown how it is the periodicity of the system which ultimately allows for an additional extraordinary transmission.
In Chapter 3 the setup used in this research will be treated. The sample under consideration and the light source that was used to illuminate the sample will receive extra attention in this chapter, as they turn out to have the largest impact on the quality of the resulting spectra.
The fourth chapter will show the results as they were obtained in this project. First numerical calculations using the theory as described in Chapter 2 will be done to determine what we expect to see from measuring EOT on the sample. After that the actual measured spectra will be shown, and finally a fitting scheme will provide us with numerics based on the measured spectra which will be compared to the calculated values from the first section.
Chapter 5 will summarize the conclusions which can be drawn from the research and corresponding analysis.
The sixth chapter, finally, will contain some outlooks on possible follow-up projects aimed at both improving the setup as was used in this research and at additional research possibilities to further increase our knowledge on the effect and behaviour of EOT.

1.2 Introducing Extraordinary Optical Transmission

In 1998, Ebbesen et al. [4] found that transmission of light through periodic hole arrays in metal films, of which the individual holes had smaller dimensions than the wavelength of the impinging light, resulted in spectra that differed from the spectrum one would expect based on aperture theory. The main difference consisted of relative high transmission peaks at certain wavelengths, with reported intensities being orders of magnitude greater [4] than what would be expected, whilst the wavelengths at which the enhanced transmissions occured seemed to depend primarily on the periodicity of the periodic array. Subsequent research on this *Extraordinary Optical Transmission* (EOT) eventually led to theories explaining EOT as resulting from coupling of the impinging light field to Surface Plasmon Polaritons (SPP's) on the metallic surface. Although the theory of this SPP coupled effect is in qualitative agreement with measured spectra, there is still a debate on the quantitative interpretation whether the SPP's should lead to either *loss channels* [3] in the transmission or to *enhanced transmission* [15] at certain wavelengths.

Apart from fundamental research on EOT, research from an applicational point of view is also done. Due to the strong dependence of the transmitted light on the local dielectric properties at the interface, one can construct highly sensitive chemical/biomedical detectors using EOT [6]. It is expected that EOT will eventually lead to the creation of cheap and easy to use disposable chemical/biomedical sensors which require only small test volumes.

The research done in this project, and as is described in this thesis, was aimed at gaining a general understanding of EOT and hands-on experience with the interaction of an incident light field with periodic aperture arrays having a specific pitch of 770 nm in thin gold films. The motivation for this specific pitch size as well as the material is based on research which will be done within this research group in the near future on optical manipulations with Rubidium atoms, requiring the incident light field to have vacuum wavelengths in the region of 770–790 nm, in the vicinity of surfaces. While generally research on EOT involves using aperture arrays which contain apertures smaller than half the wavelength of the incident light, the apertures that were used in this research ranged in size from sub wavelength sized up to apertures slightly larger than the shortest wavelength of the incident light field.

Chapter 2

Theory

In this chapter an overview of theoretical elements required to understand EOT will be treated. First the general theory of transmission through small apertures will be explained. In the second section the relevant behaviour of metals when subjected to an incident light field and the coupling of light to Surface Plasmons is treated. Section 2.3 combines the results from the first two sections, adding periodicity of the apertures as an extra ingredient, to show how EOT spectra can be qualitatively understood.

2.1 Aperture Theory

When looking at the light intensity being transmitted through a circular hole in a conducting film, it is geometrically expected that the total power being able to pass through the hole to scale with the area of the hole $P = \pi a^2 I \sim a^2$, with I being the incident intensity (power per unit area) and a being the radius of the hole. In this case it is immediately seen that the intensity scales independently of the wavelength of the incident field. This is correct when looking at aperture sizes much larger than the typical wavelength of the incident light. When however the apertures become small with respect to the typical wavelength of the incident light, this simple geometric result is no longer valid as can be shown in the following qualitative way. Consider what would happen when a light field would try to pass a hole in a conductor with a holesize of either the same size as the wavelength of the incident light or a holesize much larger than the wavelength of the incident light. In the first case, the electric field will induce a charge seaparation in the walls of the hole, which in turn will influence the light field within the hole. As the hole diameter is of the order of the wavelength of the incident light, this effect can be expected to influence, and be influenced by, *all* the light within the hole. If on the other hand the hole is large with respect to the wavelength of the incident light, this distortion will at best have an effect on the light field near the walls of the hole while the bulk of the incident light

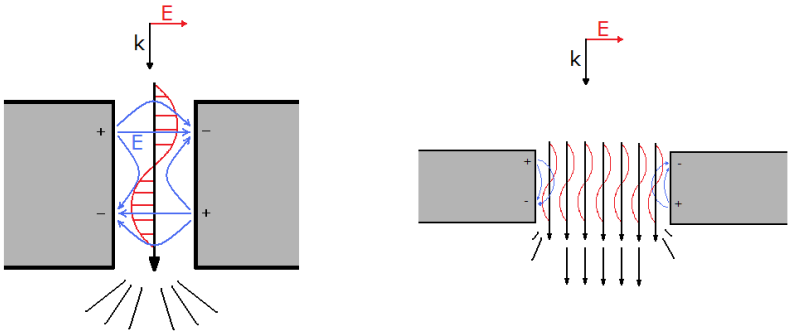

Figure 2.1.1: Qualitative description of the difference between small holes versus large holes in the case of transmission. In the left picture all the light which travels through a small hole is influenced by the induced charge separation. In the right picture the hole is made much larger than the wavelength of the incident light and the bulk of the light is no longer influenced by the surface charges at the hole walls. Red indicates the direction of the electric field from the passing light while blue denotes the induced electric field from the metallic wall.

will pass through the hole without ever noticing it was a hole in the first place, as shown in Figure (2.1.1). As the effect as described above depends on the ratio of the aperture size and the specific wavelength of the light that is being used, it follows that the fraction of the transmitted intensity will depend on the wavelength of the incident light. Bethe [1] showed, already in 1944, that for a small aperture ($a \ll \lambda$) in a perfectly conducting medium the transmitted power is indeed dependent on the wavelength of the impinging light. For circular apertures with radius a Bethe found the effective aperture size, which allows for calculating the total transmission in the same way as in the previous case, depended on the actual aperture size and wavelength of the incident light according to

$$A_{\perp} = \frac{64}{27\pi} k^4 a^6 \tag{2.1}$$

With k being the absolute value of the wavevector of the incident light and $A_{\perp}$ the effective aperture size when assuming orthogonal incidence of the light field. As one can immediately see, the total transmitted power is strongly determined not only by the effective hole size, which now scales as the sixth power of the actual hole radius, but the fourth power dependence on the wavelength ($\lambda = \frac{2\pi}{|k|}$) now plays an important role as well.

2.2 Surface Plasmon Polaritons

2.2.1 Plasmons

The high electric conductivity of a metal is the result of the mobility of the individual electrons within a metal. The tremendous amount of con-

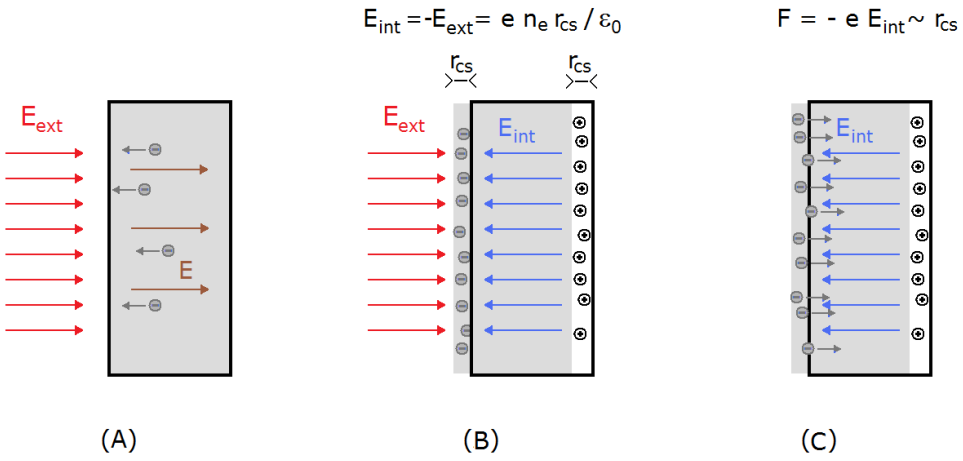

Figure 2.2.1: Charge separation in a metal due to an external electric field E_{ext}. (A) An external electric field E_{ext} induces a charge separation in the metal. (B) In the steady state situation the charge separation will compensate the external field inside the metal by creating an electric field $E_{\text{int}} = -E_{\text{ext}}$. (C) When the external field is switched off, the electron cloud will start accelerating due to E_{int}. The electron motion decreases the charge surplus, leading to a linear dependence of the internal electric field on the charge separation distance $F \sim E_{\text{int}} \sim -r_{\text{cs}}$.

duction electrons present in metals, with electron densities of the order of $n_{\text{e}} \sim 10^{28}\,\text{m}^{-3}$, allows for treating the electrons as one homogeneously distributed charge density $\rho_{\text{e}} = e\,n_{\text{e}}$ which is located around and throughout a static background lattice of positive ions. Due to the electric forces between the positive ion background and the negative charge cloud, the charge centers of the cloud and the background are always kept at the same place, as long as there is no external force (electric field) enforcing a charge separation. When such an external field E_{ext} *is* present, however, the mobility of the negative charge cloud will lead to a charge separation over a distance r_{cs} with a resulting electric field $E_{\text{cs}} = \epsilon_0^{-1}\rho_{\text{e}} r_{\text{cs}}$ that will negate the effects of the externally applied electric field within the conductor, see Figure (2.2.1). When the external electric field is subsequently switched off, the displaced electron cloud will be accelerated by the remaining electric field that resulted from the charge separation and will initially be subject to a force

$$\begin{aligned} F_{\text{e}} &= -eE_{\text{cs}} \\ &= \frac{-e(en_{\text{e}})r_{\text{cs}}}{\epsilon_0} \\ &= m_{\text{e}}\frac{\mathrm{d}^2 r}{\mathrm{d}t^2}. \end{aligned} \tag{2.2}$$

As initially both the variable r and the initial r_{cs} refer to the same position of the electron cloud with respect to the ion lattice, r_{cs} can be considered an

initial condition for r when rewriting the previous formula and recognizing it to be a harmonic oscillator, see for example Jackson [7] or Kittel [8]

$$\begin{aligned}
\frac{-e(en_\mathrm{e})r}{\epsilon_0} &= m_\mathrm{e}\frac{\mathrm{d}^2 r}{\mathrm{d}t^2} \quad \Leftrightarrow \\
\frac{-e^2 n_\mathrm{e}}{\epsilon_0 m_\mathrm{e}}\, r &= \frac{\mathrm{d}^2 r}{\mathrm{d}t^2} \quad \Leftrightarrow \\
r(t) &= r_0 e^{i\omega_\mathrm{p} t} \\
\text{with} \quad r_0 = r_\mathrm{cs} \quad &\text{and} \quad \omega_\mathrm{p} = \sqrt{\frac{e^2 n_\mathrm{e}}{\epsilon_0 m_\mathrm{e}}},
\end{aligned} \tag{2.3}$$

where ω_p is the plasma frequency, i.e. the frequency at which the free electron cloud, which can be considered a plasma, inside the metal oscillates around the positive ion lattice when there is no external force acting on the electrons. At the surface of the metal, where the electron cloud experiences the metal as being only a half-space of ions, the net force on the electron cloud as used in Equation (2.2) is also halved, leading to a surface plasma frequency of

$$\begin{aligned}
\omega_\mathrm{sp} &= \sqrt{\frac{e^2 n_\mathrm{e}}{2\epsilon_0 m_\mathrm{e}}} \\
&= \frac{1}{\sqrt{2}}\omega_\mathrm{p}.
\end{aligned} \tag{2.4}$$

The direct importance of these plasma frequencies is that for applied oscillating electric fields, i.e. incident light, the electron cloud in the metal will not allow propagation through the metal when the frequency of the oscillation lies below these plasma frequencies. In this case the external field will be varying slowly enough for the electrons in the metal to create a charge separation in the metal thus negating the electric field. As the incident field oscillation surpasses the plasma frequency the electron plasma will no longer be able to fully compensate the electric field throughout the metal and the metal will become transparent, although attenuating near the plasma frequency.

When exciting an electron plasma, thus creating plasma oscillations, these oscillations are quantized in units of the plasma frequency with corresponding energies of $\hbar\omega_\mathrm{p}$ for a volume oscillation and $\hbar\omega_\mathrm{sp}$ for a surface oscillation respectively. These quanta of plasma oscillations are referred to as either Bulk Plasmons or Surface Plasmons.

2.2.2 Coupling Light to Surface Plasmons

When Surface Plasmons are present on a metallic surface, an impinging light field which cannot penetrate the metal *can* couple to a Surface Plasmon thus leading to a travelling charge density wave along the surface which is called

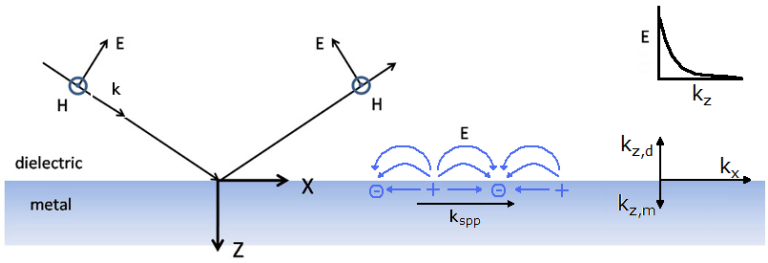

Figure 2.2.2: Creation of a SPP by incident light on a metal surface, taken from WEINER [16] (and modified). When incident light on a surface couples to a Surface Plasmon, it can lead to a travelling charge density disturbance along the surface, a SPP. This SPP has a definite direction in which it is travelling ($\hat{k}_{\text{SPP}} = \hat{k}_x$) as well as two orthogonal imaginary components $k_{(z,d)}$, $k_{(z,m)}$, which manifest as an evanescent electric field in both the dielectricum and the metallic volume.

a Surface Plasmon Polariton (SPP). In this section it will be shown how, starting out from the MAXWELL's equations, SPP properties can be related to the properties of the incident photon that coupled to the Surface Plasmon.

Taking the MAXWELL's equations in the absence of a free charge density or current density,

$$\nabla \cdot \vec{E} = 0 \qquad \text{and} \quad \nabla \times \vec{E} = -\mu_0 \frac{\partial \vec{H}}{\partial t} \tag{2.5}$$

$$\nabla \cdot \vec{H} = 0 \qquad \text{and} \quad \nabla \times \vec{H} = \epsilon \frac{\partial \vec{E}}{\partial t}, \tag{2.6}$$

we can investigate what happens when an incident light field impinges on a metal surface as is depicted in Figure (2.2.2). The incident field with $|\vec{k}_0| = \frac{\omega}{c}$ consists of oscillating electric and magnetic field components related to the frequency ω and the corresponding $\vec{k}$ vector through

$$\vec{E} = \vec{E}_0 e^{i(\vec{k}\cdot\vec{r}-\omega t)} \tag{2.7}$$

$$\vec{H} = \vec{H}_0 e^{i(\vec{k}\cdot\vec{r}-\omega t)}, \tag{2.8}$$

in which $\vec{E}\cdot\vec{H} = \vec{E}\cdot\vec{k} = \vec{H}\cdot\vec{k} = 0$ as light is a travelling transversal electromagnetic field. Assuming the same vectorial decomposition as is depicted in Figure (2.2.2), i.e. the metal surface lies in the (x,y) plane, the impinging light $\vec{k}$ travels in the (x,z) plane and the magnetic field points in the $\hat{y}$ direction, Equations (2.7) and (2.8) can be simplified, as in that case $\vec{E}_0 = (E_{(0,x)},0,E_{(0,z)})$ and $\vec{H}_0 = (0,H_{(0,y)},0)$, while $\vec{k} = (k_x,0,k_z)$. Combining

in this case the Equations (2.7) and (2.8) with Equations (2.6) then gives

$$\begin{aligned}
\nabla \times \vec{H} &= -\frac{\partial H_y}{\partial z}\hat{x} + \frac{\partial H_y}{\partial x}\hat{z} \\
&= (-ik_z, 0, ik_x) \cdot H_{(0,y)} e^{i(k_x x + k_z z - \omega t)} \\
&= \epsilon \frac{\partial \vec{E}}{\partial t} \\
&= (-i\omega\epsilon E_{(0,x)}, 0, -i\omega\epsilon E_{(0,z)}) \cdot e^{i(k_x x + k_z z - \omega t)} \quad \Leftrightarrow \\
k_z H_y = \epsilon\omega E_x \quad &\text{and} \quad k_x H_y = -\epsilon\omega E_z, \qquad (2.9)
\end{aligned}$$

which must be satisfied at both sides of the dielectric-metal interface.

The continuity of the MAXWELL's equation at the surface of the metal, in the case depicted in Figure (2.2.2), requires the electric and magnetic field near the surface to satisfy,

$$\left.\begin{array}{rl} H_{(d,x)} & = 0 = H_{(m,x)} \\ H_{(d,y)} & = H_{(m,y)} \\ H_{(d,z)} & = 0 = H_{(m,z)} \end{array}\right\} \qquad (2.10)$$

and

$$\left.\begin{array}{rl} E_{(d,x)} & = E_{(m,x)} \\ E_{(d,y)} & = 0 = E_{(m,y)} \\ \epsilon_d E_{(d,z)} & = \epsilon_m E_{(m,z)} \end{array}\right\} \qquad (2.11)$$

where subscripts m and d refer to the metallic resp. dielectric side of the interface. Combining Equations (2.9) with the continuity requirements (2.10) and (2.11), and noting that inside the metal the z component of $\vec{k}$ is inverted $\hat{k}_{m,z} = -\hat{k}_{d,z}$[1], the requirements which must be satisfied at the interface of the metal become

$$\begin{aligned}
\frac{k_{(d,z)} H_{(d,y)}}{\epsilon_d \omega} &= E_{(d,x)} = E_{(m,x)} = \frac{-k_{(m,z)} H_{(m,y)}}{\epsilon_m \omega} \quad \Leftrightarrow \\
\frac{k_{(d,z)}}{\epsilon_d} &= \frac{-k_{(m,z)}}{\epsilon_m} \qquad (2.12) \\
\frac{k_{(d,x)} H_{(d,y)}}{-\omega} &= \epsilon_d E_{(d,z)} = \epsilon_m E_{(m,z)} = \frac{k_{(m,x)} H_{(m,y)}}{-\omega} \quad \Leftrightarrow \\
k_{(d,x)} &= k_{(m,x)} \,. \qquad (2.13)
\end{aligned}$$

[1] Consider a SPP travelling along the surface; the component of k_{SPP} parallel to the surface will on both the dielectric and the metal side of the interface be pointing in the same direction, but the perpendicular components of k_{SPP} must necessarily be opposite $\hat{k}_{d,z} = -\hat{k}_{m,z}$ as the half-spaces containing the metal and the dielectricum are on the opposite side of the SPP. If the perpendicular components would not be opposite, it would require the dielectricum and the metal to occupy the *same* half-space as both z components would be pointing in the same direction.

As both the k vectors in the metal k_m and in the dielectricum k_d are related to the corresponding vacuum vector k_0 through $k_d^2/\epsilon_d = k_0^2 = k_m^2/\epsilon_m$, this relation can be combined with Equations (2.12) and (2.13) to acquire

$$\begin{aligned}
\frac{k_d^2}{\epsilon_d} &= \frac{k_{(d,x)}^2 + k_{(d,z)}^2}{\epsilon_d} = k_0^2 \quad \Leftrightarrow \\
k_{(d,x)}^2 &= \epsilon_d k_0^2 - k_{(d,z)}^2 \\
&= \epsilon_d k_0^2 - \frac{\epsilon_d^2}{\epsilon_m^2} k_{(m,z)}^2 \\
&= \epsilon_d k_0^2 - \frac{\epsilon_d^2}{\epsilon_m^2}(\epsilon_m k_0^2 - k_{(m,x)}^2) \\
&= \epsilon_d k_0^2 - \frac{\epsilon_d^2}{\epsilon_m} k_0^2 + \frac{\epsilon_d^2}{\epsilon_m^2} k_{(m,x)}^2 \quad \Leftrightarrow \\
k_{(d,x)}^2 \left(1 - \frac{\epsilon_d^2}{\epsilon_m^2}\right) &= \left(\frac{\epsilon_d \epsilon_m^2}{\epsilon_m^2} - \frac{\epsilon_d^2 \epsilon_m}{\epsilon_m^2}\right) k_0^2 \quad \Leftrightarrow \\
k_{(d,x)}^2 &= k_0^2 \left(\frac{\epsilon_d \epsilon_m^2}{\epsilon_m^2} - \frac{\epsilon_d^2 \epsilon_m}{\epsilon_m^2}\right) / \left(\frac{\epsilon_m^2}{\epsilon_m^2} - \frac{\epsilon_d^2}{\epsilon_m^2}\right) \\
&= k_0^2 \frac{\epsilon_d \epsilon_m (\epsilon_m - \epsilon_d)}{(\epsilon_m - \epsilon_d)(\epsilon_m + \epsilon_d)} \\
&= k_0^2 \frac{\epsilon_d \epsilon_m}{\epsilon_m + \epsilon_d},
\end{aligned}$$

which, when taking the square root of both sides and noting that, as SPP's are necessarily bound to the interface and thus giving $k_{d,x} = k_{\text{SPP}}$, results in the following SPP relation at the surface of a metal. See also WEINER [16] or ZAYATS [17] for slightly different derivations leading to the same results.

$$k_{\text{SPP},x} = k_0 \sqrt{\frac{\epsilon_d \epsilon_m}{\epsilon_m + \epsilon_d}} \tag{2.14}$$

From this, it can be directly deduced that, for $\epsilon_d \approx 1$ and $\epsilon_m \ll -1$, the SPP wavelength, $\lambda_{\text{SPP}} \sim k_{\text{SPP}}^{-1}$ will always be smaller than the corresponding vacuum wavelength of light.

In real metals ϵ_m is always both complex (the real part being negative) and frequency dependent, $\epsilon_m \Rightarrow \epsilon_m(\omega) \in \mathbb{C}$, leading to a complex k_{SPP} as well. The real part of k_{SPP} then gives the energy and direction, while the imaginary part gives a measure of the amount of damping the SPP is confronted with. When defining the energy propagation length L_{SPP} as the distance after which the energy of the SPP has been reduced by a factor of $\frac{1}{\text{e}}$ and noting that the total energy U stored in a SPP is directly related to the square of the electric field vector, we can determine the energy propagation

length using, assuming the SPP to be travelling in the x direction,

$$\begin{aligned} U &\sim |\vec{E}|^2 \\ &= E_0^2\, e^{2i(k_{\text{SPP}}x-\omega t)} \\ &= E_0^2\, e^{2i(\text{Re}[k_{\text{SPP}}]x-\omega t)}\, e^{2i^2\,\text{Im}[k_{\text{SPP}}]x} \\ &= e^{-2\,\text{Im}[k_{\text{SPP}}]x} \cdot E_0^2\, e^{2i(\text{Re}[k_{\text{SPP}}]x-\omega t)}, \end{aligned}$$

which, when requiring the decaying exponential in the last line to become $\frac{1}{\text{e}}$ directly yields

$$\begin{aligned} e^{-1} &= e^{-2\,\text{Im}[k_{\text{SPP}}]x} \quad \Leftrightarrow \\ L_{\text{SPP}} &= x = \frac{1}{2\,\text{Im}[k_{\text{SPP}}]}. \end{aligned} \tag{2.15}$$

SPP's travelling along a surface extend in the direction perpendicular to the surface as well. This extension manifests itself as an evanescent field penetrating in both the metal and the dielectric region, although penetration in the metal is strongly attenuated, as the frequency of the photon that coupled into the SPP is necessarily below the plasma frequency. Using a similar argument as the calculations that led to Equation (2.15), i.e. by replacing $k_{\text{SPP}}x$ with $k_{(d,z)}z$ for the dielectric or $k_{(m,z)}z$ for the metal, it is possible to calculate the penetration depth of the square of the evanescent field in the dielectric and metal region,

$$\begin{aligned} \delta_{\text{E},m} &= \frac{1}{2\,\text{Im}[k_{(m,z)}]} \\ \delta_{\text{E},d} &= \frac{1}{2\,\text{Im}[k_{(d,z)}]} \end{aligned}$$

where δ_{E} denotes the typical penetration depth of the square of the evanescent field in the metallic and dielectric region. Using Equation (2.14) together with the rquirement of energy conservation, $k_{\text{SPP},x}^2 + k_z^2 = \epsilon k_0^2$, immediately gives for the z components of k_{SPP}

$$\begin{aligned} k_{(d,z)}^2 + k_{\text{SPP},x}^2 &= \epsilon_d k_0^2 \Leftrightarrow \\ k_{(d,z)} &= k_0 \sqrt{\epsilon_d - \frac{\epsilon_d \epsilon_m}{\epsilon_d + \epsilon_m}} \\ &= k_0 \sqrt{\frac{\epsilon_d(\epsilon_d + \epsilon_m) - \epsilon_d \epsilon_m}{\epsilon_d + \epsilon_m}} \\ &= k_0 \sqrt{\frac{\epsilon_d^2}{\epsilon_d + \epsilon_m}} \end{aligned} \tag{2.16}$$

and

$$
\begin{aligned}
k_{(m,z)}^2 + k_{\text{SPP},x}^2 &= \epsilon_m k_0^2 \Leftrightarrow \\
k_{(m,z)} &= k_0 \sqrt{\epsilon_m - \frac{\epsilon_d \epsilon_m}{\epsilon_d + \epsilon_m}} \\
&= k_0 \sqrt{\frac{\epsilon_m(\epsilon_d + \epsilon_m) - \epsilon_d \epsilon_m}{\epsilon_d + \epsilon_m}} \\
&= k_0 \sqrt{\frac{\epsilon_m^2}{\epsilon_d + \epsilon_m}}. \qquad (2.17)
\end{aligned}
$$

When assuming the real part of ϵ_m to satisfy the relation $\text{Re}[\epsilon_m] \ll -\epsilon_d$, which is the case for real metals, the denominators in the square roots in Equations (2.16) and (2.17) become negative, thus leading to imaginary results for both $k_{(d,z)}$ and $k_{(m,z)}$. The $\frac{1}{\text{e}}$ decay length of the square of the evanescent field in both media can then be directly calculated to equal

$$
\begin{aligned}
\delta_{\text{E},m} &= \frac{1}{2\,\text{Im}[k_{(m,z)}]} \\
&= \frac{1}{2k_0\,\text{Im}[\sqrt{\epsilon_m^2/(\epsilon_d + \epsilon_m)}]} \\
&= \frac{\lambda_0}{4\pi}\,\text{Im}\left[\sqrt{\frac{\epsilon_d + \epsilon_m}{\epsilon_m^2}}\right] \\
&\approx \frac{\lambda_0}{4\pi\sqrt{|\epsilon_m|}} \qquad (2.18) \\
\delta_{\text{E},d} &= \frac{1}{2\,\text{Im}[k_{(d,z)}]} \\
&= \frac{1}{2k_0\,\text{Im}[\sqrt{\epsilon_d^2/(\epsilon_d + \epsilon_m)}]} \\
&= \frac{\lambda_0}{4\pi}\,\text{Im}\left[\sqrt{\frac{\epsilon_d + \epsilon_m}{\epsilon_d^2}}\right] \\
&\approx \frac{\lambda_0}{4\pi}\sqrt{\frac{|\epsilon_m|}{\epsilon_d^2}} \qquad (2.19)
\end{aligned}
$$

where the approximations are based on the notion that $\text{Re}[\epsilon_m] \ll -\epsilon_d$. The importance of this penetration effect of the SPP lies in direct coupling between two sides of a thin metal film. If the thickness of a metal film would be on the order of the skin depth of the evanescent field in the metal, any SPP travelling over the surface on one side would extend through the film to the other side, where, by direct coupling with Surface Plasmons, it could scatter into a SPP mode on that side.

2.3 Periodic Structures and Transmission

Combining the results from the preceding sections and applying it to periodic arrays of sub wavelength apertures the wavelength dependence of EOT can be clarified. For this, first periodic structures and resonance conditions will be treated. After that interference of different transmission channels will be considered and in the final section the RAYLEIGH anomaly, often seen in transmission through aperture arrays, will be treated.

2.3.1 Resonance Conditions

When a metallic surface contains a two dimensional square periodic structure of apertures, any travelling SPP will periodically couple to an aperture, allowing it to either scatter into another SPP mode (for a thin metallic film this includes scattering to a SPP mode on the other side of the film) or scatter into the light field. If the amount of SPP's traversing the surface is large enough for the SPP's to interfere with each other when scattering off the apertures, it becomes possible to treat the scattering of SPP's as a two dimensional crystallographic scattering problem. For a spectrum of k_{SPP}'s, the LAUE equations can be used to determine which wavevectors will be able to constructively interfere with one another upon scattering off an aperture array. These LAUE conditions are, in two dimensions, given by (see ZAYATS [17] or KITTEL [8])

$$k_{\text{SPP}} = \pm p \frac{2\pi}{P} \vec{u}_1 \pm q \frac{2\pi}{P} \vec{u}_2, \tag{2.20}$$

in which P is the pitch of the lattice, $\vec{u}_1$ and $\vec{u}_2$ are the reciprocal lattice vectors ($\vec{u}_1 \cdot \vec{u}_2 = 0$ for a square lattice) and p and q are integers.

Since SPP's are created by shining light on the metal surface at a nearly orthogonal incidence, it is not known a priori what the direction of k_{SPP} will be. However, as the absolute value of k_{SPP} is directly related to the wavelength of the incident light, which can be seen by combining $\lambda_0 = 2\pi/|k_0|$ with Equation (2.14), the LAUE conditions can be satisfied whenever, assuming positive indices pq and orthonormal reciprocal lattice vectors $\vec{u}_1$

and $\vec{u}_2$,

$$\begin{aligned}
|k_{\text{SPP}}| &= \sqrt{p^2\frac{(2\pi)^2}{P^2}\vec{u}_1\cdot\vec{u}_1 + q^2\frac{(2\pi)^2}{P^2}\vec{u}_2\cdot\vec{u}_2 + 2pq\frac{(2\pi)^2}{P^2}\vec{u}_1\cdot\vec{u}_2} \\
&= \frac{2\pi}{P}\sqrt{p^2+q^2} \\
&= |\vec{k}_0|\sqrt{\frac{\epsilon_m\epsilon_d}{\epsilon_m+\epsilon_d}} \qquad \text{(equation 2.14)} \qquad \Leftrightarrow \\
\frac{2\pi}{P}/|\vec{k}_0| &= \sqrt{\frac{\epsilon_m\epsilon_d}{\epsilon_m+\epsilon_d}}/\sqrt{p^2+q^2} \qquad \Leftrightarrow \\
\lambda_0 &= P\sqrt{\frac{1}{p^2+q^2}\frac{\epsilon_m\epsilon_d}{\epsilon_m+\epsilon_d}}. \qquad (2.21)
\end{aligned}$$

For a given array with periodicity P, SPP's will lead to a resonant effect on a metallic surface whenever the incident light has a free space wavelength λ_0 satisfying this equation.

Although the SPP's satisfying Equation (2.21) all have the same phase when coupling to an aperture, this phase is not necessarily equal to the phase of the direct transmitted light. Upon coupling to a transmission channel at the apertures, (the light from) a SPP will constructively interfere with other SPP mediated light but the interference with the direct transmitted light might lead to destructive interference and will therefore not necessarily lead to an *enhanced* transmission. Also, SPP's created by an incident light field of which the wavelength does not satisfy Equation (2.21) will still be able to lead to an additional transmission through coupling with apertures. However, as these SPP's do not satisfy Equation (2.21) their phases are not matched and the total additional transmitted intensity will be much less than in the case of SPP's satisfying Equation (2.21).

2.3.2 Interference

The total transmission of a periodic array, near the wavelength where Equation (2.21) is satisfied, depends on the interference of the SPP mediated transmission with the direct transmission through the apertures. In general when two oscillating electric fields (light) are interfering, the total intensity of the fields can be determined by addition of the electric fields still containing the phase information and determining the norm of the sum. As the total intensity is dependent on the square of the electric fields,

$$\begin{aligned}
I_{\text{tot}} &= \frac{1}{2}\epsilon_0\,|E|^2 \\
&= \frac{\epsilon_0}{2}\,(\vec{E}_{\text{dt}} + \vec{E}_{\text{SPP}})\cdot(\vec{E}^*_{\text{dt}} + \vec{E}^*_{\text{SPP}}) \\
&= \frac{\epsilon_0}{2}\,(|E_{\text{dt}}|^2 + |E_{\text{SPP}}|^2 + \vec{E}_{\text{SPP}}\cdot\vec{E}^*_{\text{dt}} + \vec{E}_{\text{dt}}\cdot\vec{E}^*_{\text{SPP}}),
\end{aligned}$$

which, when assuming $\vec{E}_{\text{SPP}}$ and $\vec{E}_{\text{dt}}$, being the electric field corresponding to the direct transmitted light, both being of the form $E_0 e^{i(\omega t+\phi_{(\text{SPP,dt})})}$, having an absolute phase of ϕ_{SPP} and ϕ_{dt} upon departure from the aperture and each having intensities $I_{\text{SPP,dt}} = \frac{\epsilon_0}{2}|E_{0,(\text{SPP,dt})}|^2$, leads to

$$\begin{aligned} I_{\text{tot}} &= I_{\text{dt}} + I_{\text{SPP}} + \frac{\epsilon_0}{2}(E_{0,\text{SPP}}E_{0,\text{dt}}e^{i(\omega t+\phi_{\text{SPP}})-i(\omega t+\phi_{\text{dt}})} \\ &\quad + E_{0,\text{dt}}E_{0,\text{SPP}}e^{-i(\omega t+\phi_{\text{SPP}})+i(\omega t+\phi_{\text{dt}})}) \\ &= I_{\text{dt}} + I_{\text{SPP}} + \sqrt{I_{\text{dt}}I_{\text{SPP}}}(e^{i(\phi_{\text{SPP}}-\phi_{\text{dt}})} + e^{-i(\phi_{\text{SPP}}-\phi_{\text{dt}})}) \\ &= I_{\text{dt}} + I_{\text{SPP}} + 2\sqrt{I_{\text{dt}}I_{\text{SPP}}}\cos(\Delta\phi) \end{aligned} \tag{2.22}$$

where $\Delta\phi$ is the phase difference between the direct transmitted light and the SPP mediated additional transmission. For real materials, where the holesize of the apertures, the free path length of the SPP's and the size of the structures are all finite, the phase difference will generally change within the bandwidth of the SPP resonance. When the intensity is assumed to have a Lorentzian shape

$$I_{\text{SPP}}(\omega) = I_{\text{SPP}}\frac{\frac{1}{4}\Gamma_{res}^2}{(\omega-\omega_{\text{res}})^2 + \frac{1}{4}\Gamma_{res}^2}, \tag{2.23}$$

in which $\omega_{\text{res}} = \frac{2\pi c}{\lambda_{(0,\text{res})}}$ depends on the resonance wavelength of the SPP mode, shown in Equation (2.21), ω is related to the vacuum wavelength of the incident light through $\omega = \frac{2\pi c}{\lambda_0}$ and Γ_{res} being the width of the resonance, the SPP mediated light will undergo a phase jump throughout the resonance given by

$$\phi_{\text{SPP}}(\omega) = \arctan\left(\frac{\omega-\omega_{\text{res}}}{\Gamma_{\text{res}}}\right) + \frac{1}{2}\pi.$$

Treating the phase of the direct transmitted light, ϕ_{dt}, which is assumed constant over the width of the SPP, as an additional phase offset for ϕ_{SPP} and which is not a priori determinable, we can assume the phase difference between SPP mediated and direct transmitted light to depend on the wavelength of the incident light as

$$\Delta\phi = \arctan\left(\frac{\omega-\omega_{\text{SPP}}}{\Gamma_{\text{SPP}}}\right) + \frac{1}{2}\pi + \phi_{\text{dt}}, \tag{2.24}$$

where the subscript *res* has been replaced with SPP to emphasize the resonance frequency and width refer to the SPP resonance.

The additional phase factor ϕ_{dt} in this formula is required to allow the phase difference between SPP mediated light and direct transmitted light to have a certain phase difference offset. In resonant processes, for example scattering of an incident light field from an atom, this additional phase

difference is essentially zero, as the incident light field and the diffracted light field start out from the same place, the atom. In the case at hand it is not necessary for this condition to hold as well, as the location where the SPP is created and the location where the SPP couples out are separated by a finite distance. In addition the coupling process of the direct transmitted light with the aperture through which it transmits can result in an extra accumulation of phase. This additional phase change due to the coupling with the aperture can also occur for the SPP, although this additional phase accumulation is not necessarily the same for both the direct transmitted and the SPP mediated light. These different processes can all lead to an additional phase offset between the SPP mediated and direct transmitted light but here they are combined in the single additional phase parameter ϕ_{dt}.

2.3.3 Rayleigh Anomaly

In addition to the effects stated in the previous paragraphs, there is another effect often seen in diffraction spectra off periodic structures called the RAYLEIGH anomaly (see RAYLEIGH [13]). The spatial distribution of light diffracted from a periodic structure consists of angularly evenly distributed successive maxima and minima resulting from constructive and destructive interference. The diffraction pattern spacing depends on the ratio between the periodicity P of the structure and the wavelength λ_{inc} of the incident light (assuming orthogonal incidence) through

$$\theta_n = \arcsin \frac{n\lambda_{\mathrm{inc}}}{P}, \tag{2.25}$$

where n is the number of the diffraction order and θ_n the corresponding angle of diffraction. For diffraction orders $n_{\max}$ resulting in maxima appearing at a grazing angle with respect to the structure, $\theta_{n_{\max}} \approx \pi/2$, the argument of the arcsin in Equation (2.25) equals 1, requiring $n_{\max}\lambda_{\mathrm{inc}}$ to be equal to the array periodicity P. In this case, shifting the wavelength of the incident light to a slightly larger wavelength will make the argument of the arcsin larger than one, which does not allow solutions to Equation (2.25), i.e. the diffraction maximum $n_{\max}$ surpasses the grating horizon and the new maximum diffraction order becomes $n_{\max} - 1$. As energy conservation requires the total diffracted energy to remain constant, this passing off of the highest diffraction order leads to a redistribution of the total diffracted energy over the remaining diffraction orders, thus increasing the intensities of the remaining orders. As such, a RAYLEIGH anomaly can be recognized by an increase in diffracted intensity whenever the wavelength of the incident light λ_{inc} becomes an integer division of the periodicity P/n.

Care must however be taken that although the anomaly itself is expected to lead to an increased transmission, the coupling of the light from the

RAYLEIGH anomaly with SPP's on the surface of a metallic array can lead to transmission effects ranging from strong enhancement to no observable effect at all. This coupling of the anomaly with SPP's is generally referred to as *Rayleigh Anomaly-Surface Plasmon Polariton Resonance*, RA-SPP, of which a nice example of the strong dependence of this RA-SPP on the properties of the dielectrica surrounding the metal film can be found in GAO [5].

Chapter 3

Experimental Setup

The measurements of EOT were done using a *Poor Man's Setup*; a cheap, small and easy to use setup that yet provided enough detail and achieved a high enough signal-to-noise-ratio to be able to do quantitative measurements on EOT. For clarity, the sample on which EOT was measured will be treated in the first section, after which in Section (3.2) a description of the setup that was used for these measurements is given. In the final section the light source will be treated in some detail, as the light source had a larger influence on the quality of the measured spectra than was anticipated.

3.1 Sample

The aperture structures that were used for EOT measurements consisted of ten square gold arrays of $50\times50\,\mu m^2$ and had square holes ranging from $160\times160\,nm^2$ to $592\times592\,nm^2$, increasing both dimensions simultaneously in steps of roughly 50 nm in between arrays. In Figures (3.1.1a) and (3.1.1b) Scanning Electron Microscope images of part of two structures are shown. In all arrays the pitch was nearly 770 nm in both directions. A full list of holesizes and periodicities is shown in Table (3.1). All gold areas had a thickness of 90 nm, were located on a glass microscope slide and were spaced 50 µm apart, see Figure (3.1.1d). For the smallest holesizes, some structures showed a lot of defects, see Figure (3.1.1c), mostly consisting of underdeveloped holes.

3.2 General Setup

The setup that was used to measure EOT consisted of a Light Emitting Diode (LED) which, using lenses and pinholes, illuminated a periodic structure on the sample. The light that was transmitted through the sample was, using more lenses and a pinhole, projected on a fiber coupler, which in turn led the transmitted spectra to an OceanOptics S2000 spectrometer

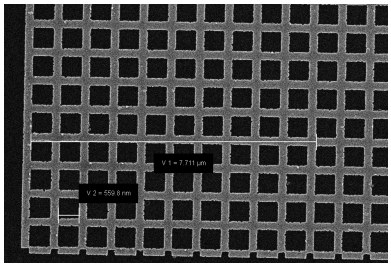

(a) Part of a structure. The measured holesize of this structure is 559.8 nm and the array pitch equals 771 nm.

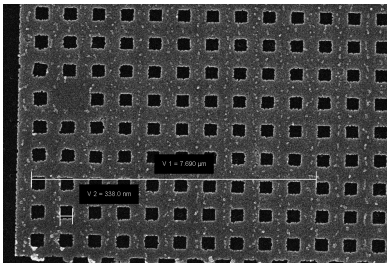

(b) Part of a structure showing one defect. The holesize and pitch are 337.9 nm and 769 nm respectively.

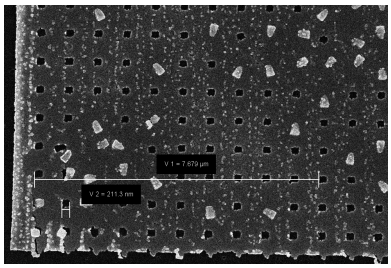

(c) A 160 nm structure rich in defects due to indeveloped holes. The white cones are gold 'bumps' stuck on the structure, presumably encapsulating a drop of photoresist.

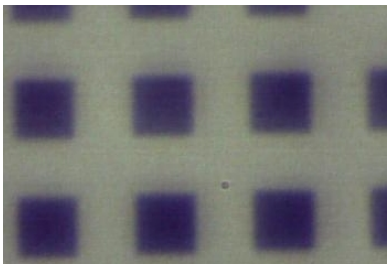

(d) Several $50\times50\,\mu m^2$ structures, backlit by a white light LED. Due to chromatic abberations the samples are slightly out of focus.

Figure 3.1.1: Optical and Scanning Electron Microscope pictures of the sample and some individual structures.

holesize [nm]	pitch [nm]
160(10)	771(3)
211(1)	767.8
253.5	773.1
306.3	765.7
337.9	768.9
401.3	769.9
433.0	771.0
485.8	771.0
570.3	771.0
591.6	771.2

Table 3.1: The aperture holesizes and periodicities of all individual structures on which EOT measurements were done. As can be seen the periodicities differ from the planned pitch of 770 nm at most by 0.6%. Measurements of the sizes were done using similar SEM pictures as shown in Figure (3.1.1).

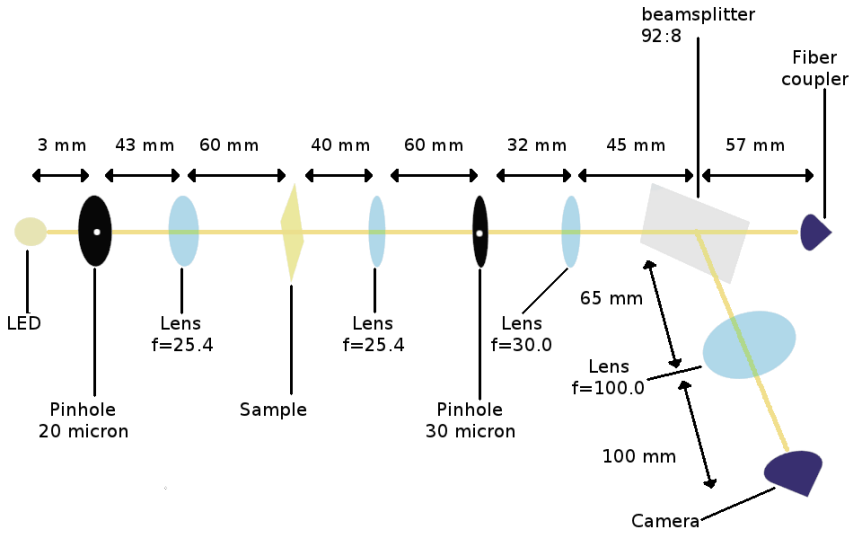

Figure 3.2.1: Overview of the setup used for measuring EOT. Distances between elements had a typical uncertainty of 1–2 mm.

for further analysis. For alignment purposes, part of the transmitted light (8%) was redirected to a camera. A schematic of the setup can be seen in Figure (3.2.1). The light of the LED first passed through a pinhole with a diameter of 30 µm to reduce the spread in incident $\vec{k}$ vectors. The image of the pinhole was in the subsequent setup treated as the lightsource. Using a lens (f=25.4 mm) that focussed the light on the sample, an illuminated spot on the sample was made with an approximate diameter of 120 µm. This allowed us to see a complete structure, including the edges of the surrounding structures, which in turn made it easier to position the structures. A second lens (f=25.4 mm) was then used to focus the light from the sample on a second pinhole, which had a diameter of 20 µm. This second pinhole served to block any light not coming from the structure under consideration. Behind the second pinhole a final lens (f=30.0 mm) was placed to collimate the remaining light prior to coupling it into a fiber. Between the last lens and the fiber coupler a beamsplitter was placed to deflect 8% of the transmitted beam off to a camera which was used for positioning and alignment purposes. The light from the setup was transported to the spectrometer using a 200 µm diameter multimode optical fiber. The spectrometer with which all measurements were done was an OceanOptics S2000 spectrometer measuring from 524 nm to 1164 nm, in 2048 steps corresponding to a resolution of 0.31 nm, and was connected to a PC using an ADC1000 USB bridge from OceanOptics.

As all the focal lengths of the lenses were given for 780 nm light, and the experiments would be conducted using light ranging from 524 nm up

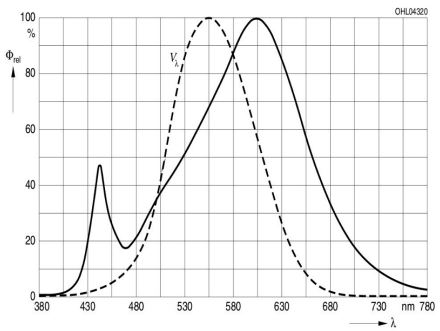

(a) LED emission spectrum, operating at 25℃ and a current of 350 mA. The dashed line V_λ shows the standard response of the human eye.

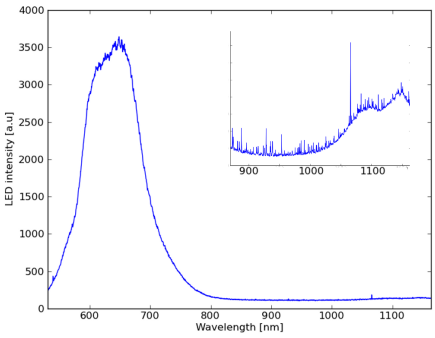

(b) Measured spectrum of the LED at 900 mA. Inset: 54× enlarged spectrum of the infrared tail.

Figure 3.3.1: LED emission spectra, as specified by the manufacturer and as measured in this experiment. Note how the measured spectrum falls off faster than the specifications give on the short wavelength side. This is expected to be due to a decreased sensitivity of the spectrometer at short wavelengths.

to 1164 nm, there would be chromatic aberrations occuring when using the white LED. To ensure good alignment the setup was back-illuminated using a LED emitting light at 760 nm and having a full width at half maximum (FWHM) of 26 nm, which was coupled directly into the fiber from the spectrometer side. Using this light all optics were aligned and positioned so that even though there would be some chromatic abberations, they would be minimized in the central spectral region of the transmission spectrum.

3.3 Light Source

The light source used to illuminate the sample was a white-light LED, type *Golden DRAGON LCW W5SM*, fabricated by OSRAM. Although the specification sheet showed only the emission spectrum in the range from 400 nm to 780 nm, as can be seen in Figure (3.3.1a), it was discovered that the LED generated an infrared tail up to (and probably beyond) 1164 nm, which was the maximum wavelength the spectrometer could measure. The measured spectrum, which is clipped by the spectrometer range, is shown in Figure (3.3.1b). As can be seen in the spectrum in Figure (3.3.1a), the LED source itself is emitting blue light at ∼440 nm which, using a fluorescent material, is absorbed and re-emitted in the range from 480 nm to 800 nm. The rise from 1000 nm onwards, see inset in Figure (3.3.1b), is not understood at the moment. Having measured a second LED from the same manufacturer having the same partnumber showed that the second LED had an infrared tail starting already at 900 nm, which might make it interesting to eventually do an extensive research on the LED emission spectra and replace the

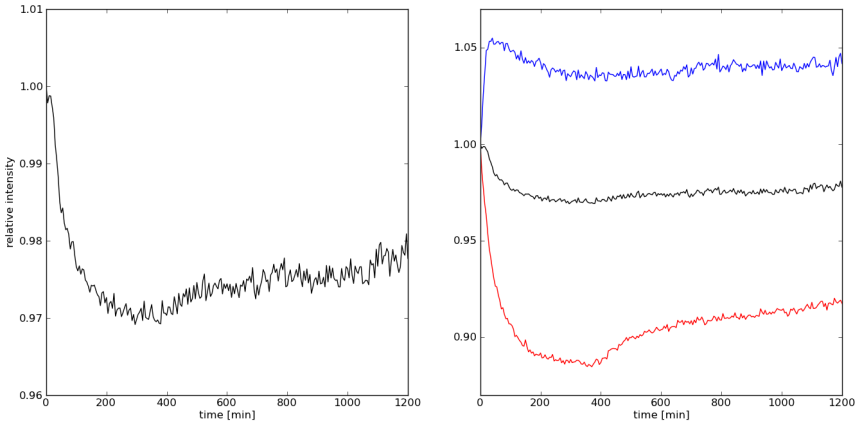

Figure 3.3.2: Temporal drift of the LED. The left graph shows the relative emitted power over time while the right graph additionally shows the power dependance over time for the two spectral windows 570 nm-620 nm (blue) and 900 nm-1100 nm (red). Note the steady increase of the infrared tail roughly five hours after switching on the LED.

current light source with a LED that produces more infrared light. During this experiment, however, the LED that has the emission spectrum as shown in Figure (3.3.1b) was used.

Ultimately the LED appeared to be a bottleneck when it came to measuring over longer periods of time. Having tried to increase the signal to noise ratio by increasing the integration time, it turned out that the total emitted power of the LED gradually decreased over time. This fall in emitted power is the result of the LED heating up, as will be shortly treated in the Outlook section (6.1), and although the details of the process through which the power drops as a function of temperature was not throroughly researched, a measurement was done on the total emitted power as a function of time to determine what the optimal measuring time would be. As can be seen in Figure (3.3.2), the measured emitted power dropped by roughly 3% in the first three hours after which the power started to slowly increase. Based on this Figure (3.3.1), all subsequent measurements were done by allowing the LED to stabilize for three hours, followed by measuring a maximum period of three hours.

Chapter 4

Results

In this Chapter the results of the EOT measurements, together with the qualitatively predicted results are reported. A fitting scheme using Python's SciPy Orthogonal Distance Regression [2] (ODR) package allowed us to quantitatively compare part of the measured EOT spectra to the calculated resonances.

4.1 Calculating the Expected Spectrum

Using the theory as was described in Chapter 2 it is in principle possible to calculate the expected transmission shape, given the material specifics, periodicity of the structure and the holesize of the apertures. In this experiment the sample in which periodic structures were made consisted of a thin gold film on a glass substrate, see Section (3.1). Applying the theory as treated in Chapter 2 to determine all characteristics gave the following results.

4.1.1 Properties of Gold

As in this experiment periodic structures in a gold film were used to produce EOT, the properties of gold will be required to calculate, using the formulas given in Chapter 2, what an EOT spectrum might look like. Using the relevant formulas from Chapter 2 the following properties of gold were determined.

Plasma Frequency

In Chapter 2, it was stated that a metal can become transparent to incident light when the frequency of the incident light is higher than the plasma frequency. To assure this does not occur in the experiment, the experiment must be done with light of a frequency below the plasma frequency of gold. The plasma frequency and corresponding surface plasma frequency

were calculated using Equation (2.4). Using for the electron density in gold n =5.9 $\times$ 10^{28} m^{-3}, which equals the atomic density in gold, this gives

- ω_p =1.37 $\times$ 10^{16} s^{-1} corresponding to a vacuum wavelength of ~140 nm,
- ω_{sp} =9.7 $\times$ 10^{15} s^{-1} corresponding to a vacuum wavelength of ~200 nm.

As long as the incident light has a corresponding vacuum wavelength significantly larger than 200 nm, the gold film will not allow direct transmission through the film. As the spectral region researched ranges from 550 nm to 1164 nm, this condition is always met.

Dielectric Constant

The dielectric constant of gold $\epsilon_m(\omega)$, which is both complex and frequency dependent, determines through Equation (2.14) what the wavelength of the SPP's will be, what the damping is the SPP's will be confronted with and how thin the gold film is allowed to be in order to prevent direct coupling through the gold film of the SPP's. Shown in Figure (4.1.1a) is the dependence of the dielectric constant on the wavelength of the incident light together with a simple polynomial fit function. The resulting parameters will allow us to calculate an estimate value for the real and imaginary part of the dielectric constant in the relevant spectral region. The dielectric constant of gold can in turn be used to calculate the dispersion relation for SPP's travelling along a gold surface by combining the dielectric constant with Equation (2.14) and noting that $\omega/|\vec{k}_0| = c$. This dispersion relation will be important in the following section where the vacuum wavelength of light will be calculated which is required to obtain a specific SPP wavelength. The dispersion relation, as calculated by using Equation (2.14), is shown in Figure (4.1.1b), both for SPP's travelling along a gold-air interface and for SPP's travelling along a gold-glass interface having a refractive index n=1.49, which is ultimately the case in this experiment. Note, however, that as the dispersion relation is calculated using the fit function as shown in Figure (4.1.1a), the dispersion curve is expected to be only correct in the spectral window ranging from 550 nm to 1200 nm.

Penetration Depth of the Evanescent Field

As was stated in Chapter 2, the penetration depth of the evanescent field determines how deep the SPP penetrates the metallic surface. In order to prevent direct coupling of SPP's through the gold film, the gold layer must be several times as thick as this depth. Since the penetration depth $\delta_{E,d}$ is inversely proportional to the square root of the dielectric constant, as can be seen in Equation (2.18), the order of magnitude of the penetration depth in the relevant spectral region can be calculated using the dielectric constant of gold at a wavelength of 550 nm. Using Equation (2.18) this leads to a

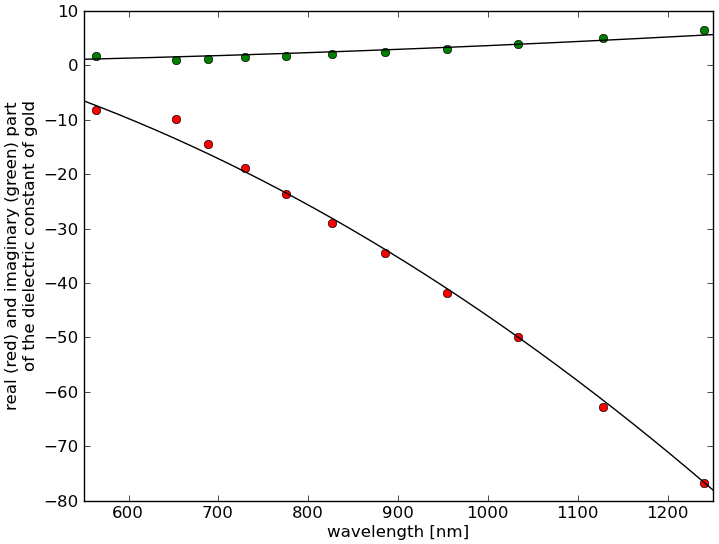

(a) Real and imaginary part of the dielectric constant of gold. The real part is strongly negative while the imaginary part is nearly constant. The measured data, taken from PALIK [11], is shown by circles while the fit functions are drawn as continuous lines.

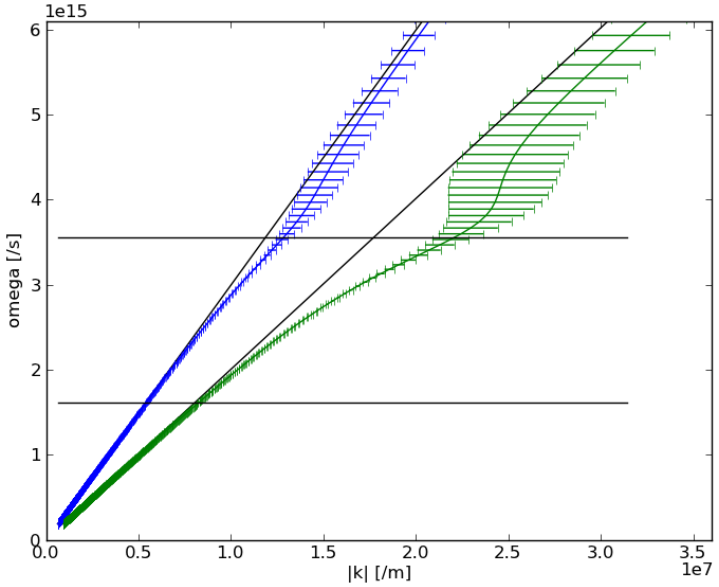

(b) Dispersion relation for SPP's travelling along a gold-air (blue) or a gold-glass (green) interface. The length of the errorbars correspond to the imaginary part of $\vec{k}$. the two black diagonal lines show the light line in the glass or air medium while the horizontal lines show the ω's corresponding to the vacuum wavelengths 550 nm and 1164 nm. Outside this window, the dispersion curve is expected to differ from the actual dispersion curve of gold.

Figure 4.1.1: Dielectric constant of gold and the corresponding dispersion relation for SPP's at a gold interface.

Index		SPP wavelength	air side		glass side	
p	q	[nm]	λ_0 [nm]	L_{SPP} [µm]	λ_0 [nm]	L_{SPP}[µm]
1	0	770.0	**787**	42.7	1179	118.8
1	1	544.5	**579**	4.3	**854**	34.7
2	0	385.0	399	0.5	**645**	8.9
2	1	344.4	352	0.5	**598**	3.9
2	2	272.2	276	0.7	511	0.6

Table 4.1: Calculated SPP resonances for a pitch of 770 nm and indices pq, see Equation(2.21), including corresponding vacuum wavelengths λ_0 and mean free paths L_{SPP} for the case of SPP's travelling along the gold-air interface (air side) and for SPP's travelling along the gold-glass interface (glass side). Higher orders for p and q are not shown as the corresponding wavelengths lie outside the region of interest. Bold numbers indicate SPP resonances that lie within the spectral window of the spectrometer.

depth of the order of 20 nm. As long as the thickness of the gold film is several times 20 nm, direct coupling through the gold film can be neglected. In the experiment this condition was satisfied as the gold film that was used had a thickness of approximately 90 nm.

4.1.2 Calculating the Resonant SPP's

Using the theory as described in Section (2.3) the SPP wavelengths which satisfy the LAUE Equations (2.20) can be determined along with the required corresponding vacuum wavelength of the incident light through Equation (2.21). In order to do this the periodicities of the structures are required to solve the LAUE Equations, after which the required incident light wavelength can be determined by using the dispersion relation as shown in Figure (4.1.1b) in combination with Equation (2.14). Considering we will only be interested in those SPP's of which the corresponding vacuum wavelength lies in the range from 550 nm to 1164 nm, and since we know the structures on the sample all have periodicities close to 770 nm, as can be seen in Table (3.1), all possible SPP resonances can be calculated as a function of the indices p and q in Equation (2.21). This directly results in the corresponding vacuum wavelengths shown in Table (4.1). As can be seen, for a hole periodicity of 770 nm we ultimately expect to see five EOT features resulting from SPP resonances.

4.1.3 Calculating the Rayleigh Anomaly

As the periodicity of the structures at hand are all the same, 770 nm, the expectation based on Equation (2.25) is that a RAYLEIGH anomaly can appear at wavelengths corresponding to an integer division of this 770 nm. As the spectral range of interest is restricted to the region 550 nm–1164 nm

there is only one anomaly, at 770 nm, as the next higher order anomaly at $\lambda = \frac{P}{2}$ =385 nm lies outside the spectral window. It is therefore expected that a RAYLEIGH anomaly will show up as an increase in overall transmittance for 770 nm and longer wavelengths.

4.1.4 Determining the Expected Spectrum

In the previous two sections the wavelengths at which both the SPP resonances as the RAYLEIGH anomaly are expected to show up were calculated. Combining these with a transmission spectrum based on BETHE's aperture theory, as is given by Equation (2.1), it is possible to determine how qualitatively an EOT spectrum is expected to look. For this qualitative determination additional assumptions are required which are stated below.

- The SPP resonances are given a width of 2% of the corresponding resonant wavelength. By setting the width at 2%, the individual peaks are still clearly visible, while the overlap with neighbouring peaks will allow for observing the effect of using an additional phase offset ϕ_{dt}, as was added to Equation (2.24).

- The SPP assisted transmission is given the same absolute intensity as the direct transmitted light. As it is unknown how for the given setup the absolute intensity of SPP mediated transmission can be calculated, the intensities are set equal thus ensuring clear peaks and dips in the spectrum without having either the SPP mediated transmission or the direct transmission dominating the spectrum.

- Only the zeroth order transmission is calculated, i.e. spatial distribution of the transmitted intensity is neglected.

Using these assumptions, a qualitative EOT transmission spectrum has been calculated and is shown in Figure (4.1.2a).

The formulas used for calculating the relative transmitted intensities, Equations (2.22), (2.23) and (2.24), contain an additional phase offset ϕ_{dt} of which the numerical value is unknown. To determine the qualitative effect of this additional phase factor, the expected spectrum is calculated for increasing phase factors ranging from no additional phase factor up to $+2\pi$, in steps of $\frac{1}{4}\pi$. The corresponding calculated spectra are shown in Figure (4.1.2b). Notice how in Figure (4.1.2a) due to interference

- the actual peak maxima are slightly shifted with respect to the calculated SPP resonance wavelengths (gray vertical lines), and

- the total transmission can become lower than one would expect based on Bethe's aperture theory (decaying gray line).

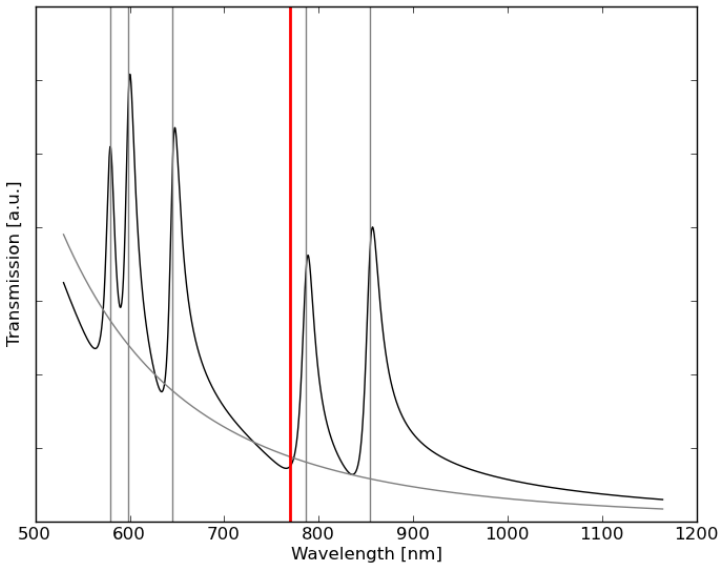

(a) Gray vertical lines show calculated SPP wavelengths. The EOT free spectrum based on BETHE's aperture theory is shown as a decaying gray line. The vertical red line indicates where we expect a RAYLEIGH anomaly to occur.

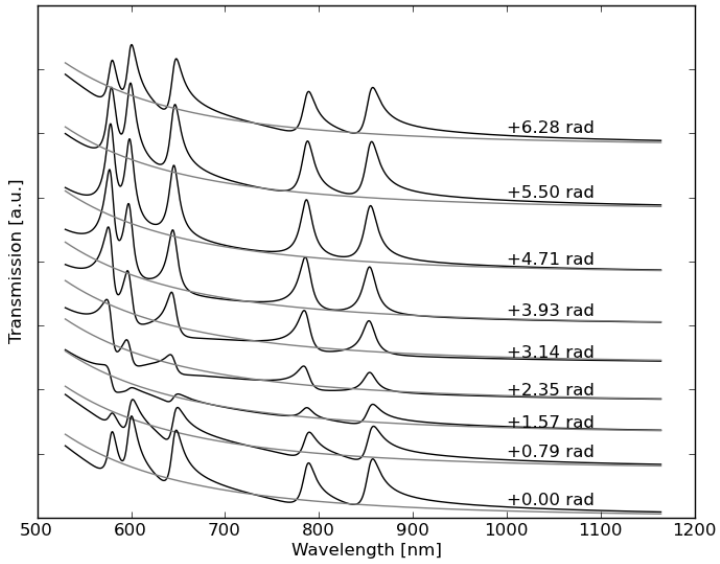

(b) Expected spectrum with an additional phase offset ϕ_{dt} ranging from 0 to 2π radians. Graphs are vertically shifted for clarity.

Figure 4.1.2: Qualitatively calculated EOT spectrum, assuming a pitch of 770 nm. (a) shows the case when there is no additional phase factor present while (b) shows the effect of an additional phase offset.

Additionally, in Figure (4.1.2b) it can be seen that the effect of adding an additional phase offset to the SPP mediated light field leads to both a change in the relative peak amplitudes and to a decrease of the overall transmission when the phase is changed up to π radians.

It should be thoroughly understood that the spectra should be considered only for their qualitative nature. The assumptions which were made in the beginning of this section were made to ensure the resulting spectrum would have clearly visible features, not to create a spectrum that would best resemble the expected spectrum (the theory to calculate a priori the complete shape and intensity of such a spectrum is not fully developed yet). The *essence* of the spectra should however be recognisable in the spectra we will ultimately measure. We can see from Figure (4.1.2) that we expect a measured spectrum to contain the following key ingredients:

- There should be a decaying backgroud.
- SPP resonances might have the position of their maximum shifted with respect to the calculated resonant wavelength.
- Resonances can lead, through interference, to a lower overall transmittance compared to what would be expected based on BETHE's aperture theory.
- Any additional phase offset might lead to additional peak modification where peaks are overlapping. In Figure (4.1.2b) the SPP's were given equal amplitudes, however there is a clear difference between the amplitudes which depends on the additional phase.
- *An* effect, probably increasing the intensity, to appear near 770 nm due to the RAYLEIGH anomaly.

4.2 Measured EOT Spectra

Using the setup as described in Chapter 3, measurements were done on the transmission of periodic arrays of subwavelength apertures in the gold film. The resulting relative transmission spectra, Figure (4.2.1), clearly show an enhancement and/or inhibition of transmission at certain wavelengths. Note on the one hand the rise of the clear peak at 800–820 nm and on the other hand the several overlapping peaks near 600 nm. In the case of the 401 nm structure there is also clearly a plateau visible near the expected RAYLEIGH anomaly at 770 nm. Although it is not very clear from the other spectra, the 306 nm, 337 nm and 433 nm structure also show some local change in the slope of the graph as shown in Figure (4.2.2a). The accompanying Figure (4.2.2b) shows a spectrum taken while the sample was slightly tilted by approximately 10 mrad, which makes the anomaly easier to see but also shifts the anomaly to a slightly different wavelength.

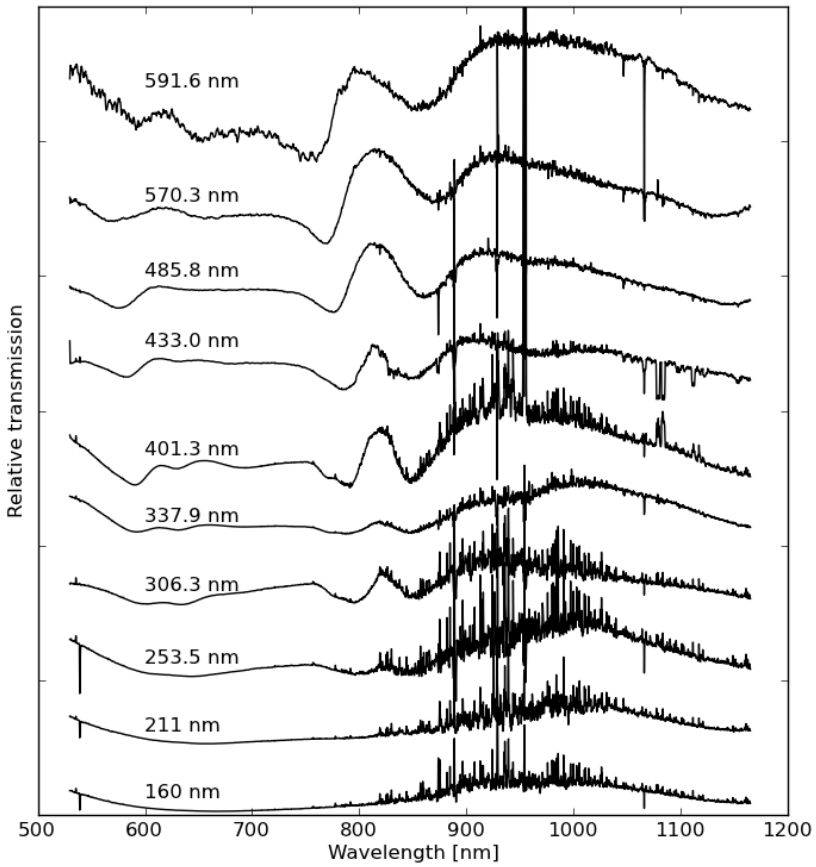

Figure 4.2.1: Measured EOT spectrum for a periodic structure on a gold film. The pitch of the structure was 770 nm, while holesizes varied from 160 nm to 592 nm, in steps of roughly 50 nm. The relative transmission is the measured transmitted intensity through the structure divided by the intensity as measured in the absence of the structure (e.g. through plain glass). Graphs have been vertically shifted for clarity.

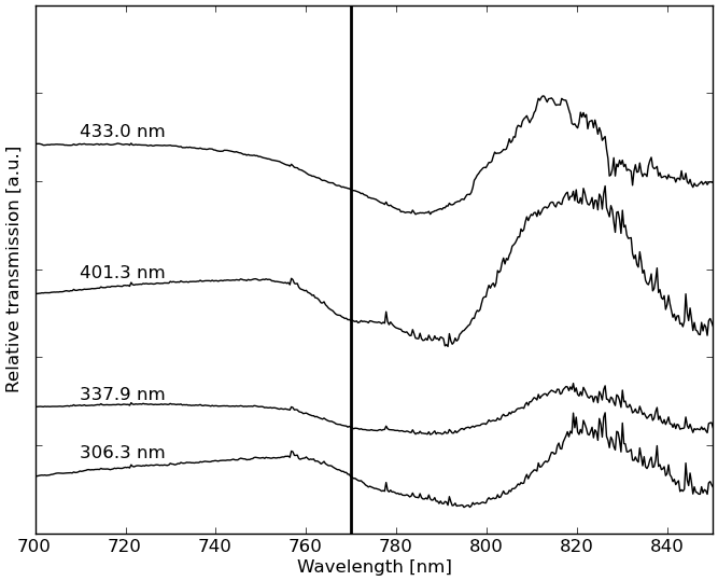

(a) RAYLEIGH anomaly in the EOT spectra of the 306(bottom)–433(top) nm structures.

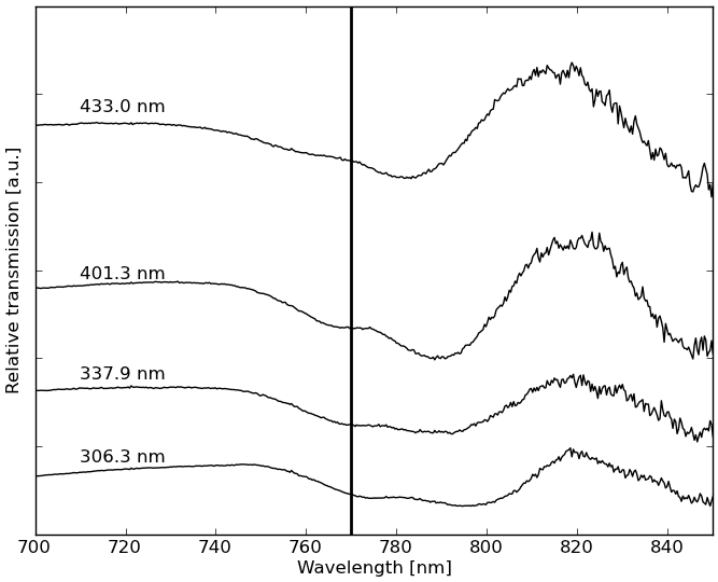

(b) RAYLEIGH anomaly as observed from a tilted sample (10 mrad). Note how in some spectra the beginning of the anomaly shifts by a few nanometer.

Figure 4.2.2: RAYLEIGH anomaly as observed in the EOT spectra. The vertical line indicates where the RAYLEIGH anomaly would be expected (770 nm).

In the spectral region from 550 nm to 850 nm, the peak and dip structures in the spectra (roughly) coincide with calculated resonance positions

as were tabulated in Table (4.1). When looking at the spectra of the 338 nm structure up to the 486 nm structure, the large infrared bump from 850 nm onwards appears to consist of two overlapping peaks. The first one corresponds to the (11) mode on the glass side, see Table (4.1), as will be shown in the next section. The second one however does not correspond to any SPP resonance as was calculated in Section (4.1.2) and it's origin is not yet understood.

4.3 Using ODR to Determine Spectra Characteristics

In the preceding two sections the expected qualitative shape of the spectrum and the spectrum as was measured were shown. Combining the predicted model with the measured spectra it is possible to determine, using a fitting scheme incorporating equations (2.22), (2.23) and (2.24) on the measured spectra, what the peak positions and phase offsets were in the measured spectra. For this the Python package for Orthogonal Distance Regression [2] (ODR) was used. Due to the numerous variables involved, four for every SPP resonance (amplitude, position, width, phase offset) and two for the corresponding background (offset and amplitude), there occurs a strong interdependence of the variables when peaks are overlapping. As can be seen in Figure (4.1.2), the three peaks near 600 nm are fairly close to one another, and as can be seen in Figure (4.2.1) there are some wide, probably overlapping, peaks present in the same region. Using the ODR routine in this region generally led to unsatisfactory fitting results comparable to those shown in Figure (4.3.1b). Using the right hand of the spectrum, in the region 750–950 nm, the fitting routine generally converged to acceptable results, an example of which can be seen in Figure (4.3.1a), returning estimates for the peak amplitudes, positions, widths and phase offsets. Of these the phase offset and the peak position of the SPP's are the parameters that purely depend on the structure under consideration. Additionally, as can be seen in Figure (4.2.1), the peak positions and relative amplitudes appear to shift when increasing the holesize. As all the spectra were fitted using the ODR routine, it is possible to determine whether this shift is an actual shift of the peak positions or a result of interference in the peak overlap. By repeatedly fitting to the measured spectra in the 750–950 nm range using slightly different starting values every time the dependence of the peak position on the holesize could be determined, as is shown in Figure (4.3.2a). The calculations from the previous section showed the peak positions are expected to be at 786.5 nm and 853.7 nm. For clarity, the numerical data that resulted from the fitting is shown in Table (4.2). The reported error margins are based on the spread in the results from the fitting routine used.

In Figure (4.3.2a) there appears a trend for the low SPP position (786.5 nm)

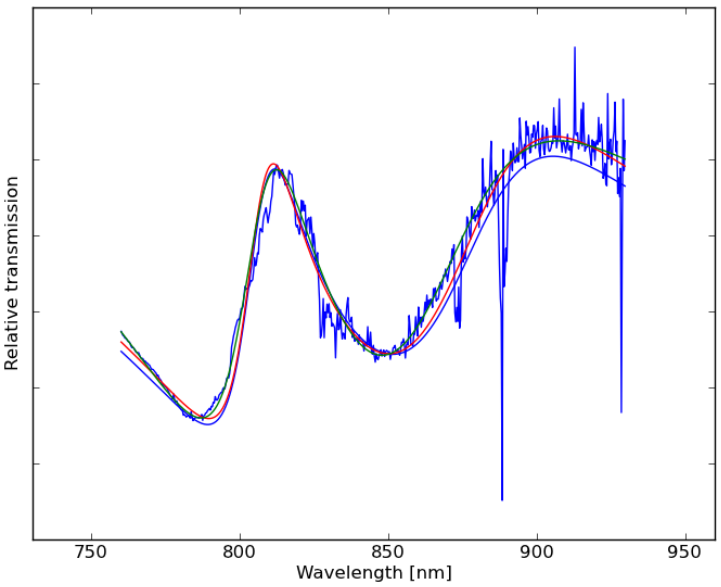

(a) Typical example of a measured EOT spectrum including fit functions which used different starting conditions to fit to the two peaks.

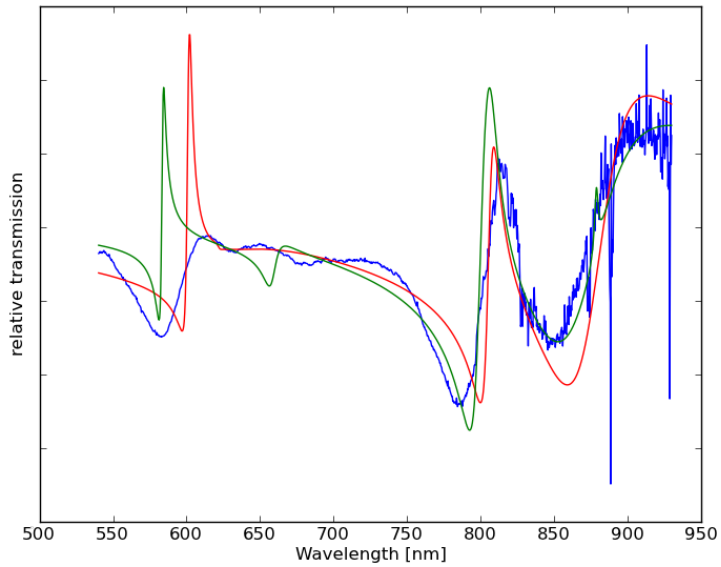

(b) Typical example of a measured EOT spectrum with a fitting scheme that included all five expected peaks.

Figure 4.3.1: Using ODR to fit to the measured EOT spectra. In both cases the spectrum was taken from the 433 nm structure, of which the full spectrum is shown in Figure (4.2.1).

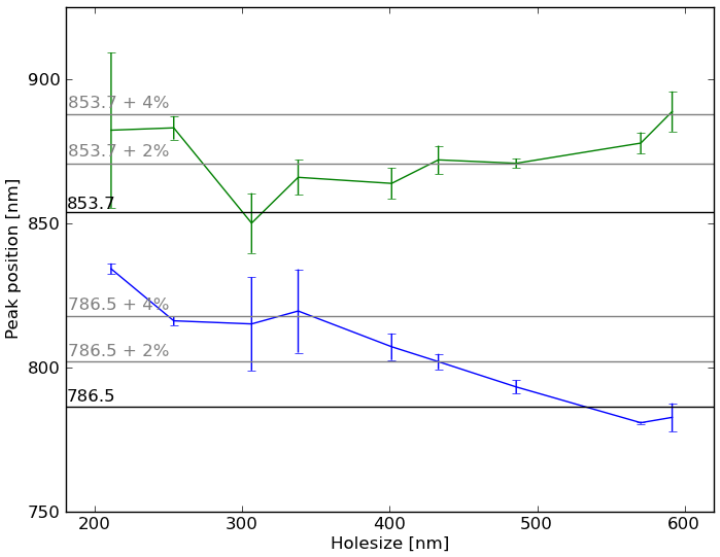

(a) Horizontal axes shows the holesize of the structure and horizontal lines in the graph give calculated expected positions (black) and redshifted positions of 2% and 4% redshifts respectively (gray).

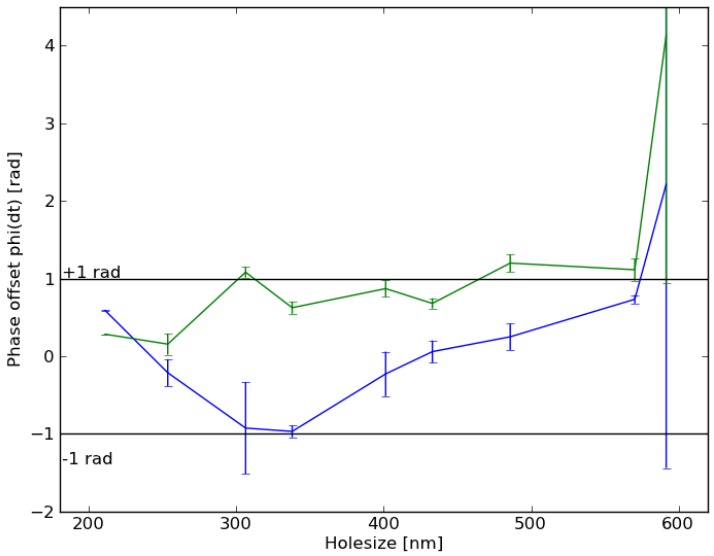

(b) The resulting phase offsets ϕ_{dt} corresponding to the peak position fits. The green graph shows the additional phase factor corresponding to the 853.7 nm SPP resonance, while the blue graph shows the required additional phase factor for the 786.5 nm SPP resonance.

Figure 4.3.2: The SPP resonance position, depending on the holesize of the structure, and the determined additional phase offset.

Holesize [nm]	Peak 1 position [nm]	Peak 2 position [nm]	ϕ_{dt} [rad] peak 1	ϕ_{dt} [rad] peak 2
211	834.1 ± 1.8	882.2 ± 26.9	0.58 ± 0.01	0.28 ± 0.01
254	816.1 ± 1.5	883.0 ± 4.0	−0.21 ± 0.17	0.15 ± 0.13
306	815.0 ± 16.1	850.0 ± 10.3	−0.92 ± 0.59	1.08 ± 0.06
338	819.5 ± 14.4	865.8 ± 6.0	−0.96 ± 0.07	0.62 ± 0.07
401	807.1 ± 4.6	863.7 ± 5.3	−0.22 ± 0.28	0.87 ± 0.10
433	801.9 ± 2.6	871.9 ± 4.9	0.05 ± 0.14	0.67 ± 0.06
486	793.1 ± 2.2	870.7 ± 1.6	0.25 ± 0.16	1.19 ± 0.11
570	780.7 ± 0.3	877.7 ± 3.7	0.73 ± 0.05	1.11 ± 0.13
592	782.6 ± 4.8	888.7 ± 6.9	2.21 ± 3.65	4.13 ± 3.19
Calculated	787	854	-	-

Table 4.2: Numerical ODR output for fitted peak positions. The last entry shows the calculated SPP positions. Reported error margins are calculated using the spread in the results from the fitting routine.

to start out at the predicted values when the holesize is 592 nm and to shift towards the red as the holesizes become smaller. This trend is not seen in the corresponding SPP mode which was expected at 853.7 nm although this peak too is systematically redshifted.

Finally in Figure (4.3.2b) the phase offset required to succesfully fit to the measured spectra is shown. As was stated in the theory chapter, a possible phase offset ϕ_{dt} was added to Equation (2.24) to account for a possible additional phase difference between the SPP mediated light and the direct transmitted light. Using the ODR fitting scheme it has been observed that not implementing this phase factor will lead to unsatisfactory results. Shown in Figure (4.3.3) is the effect of allowing or denying this extra phase offset to be implemented by the fitting routine. Figure (4.3.3a) shows the fit results when a free phase addition was allowed, while Figure (4.3.3b) shows the ODR fitting results to the exact same dataset with the exact same starting parameters, but with the additional phase offset ϕ_{dt} forced to zero.

4.4 Comparing the Redshift with Results in Literature

The resulting redshifts of the peak position as shown in the previous section have been determined by fitting to the measured spectra several times using different starting conditions. Although changing the starting conditions when fitting to the measured spectra did lead to slightly different results, the error bars in Figure (4.3.2a) were based on the spread in these different results, the general trend was definitely a redshifting for smaller holes in

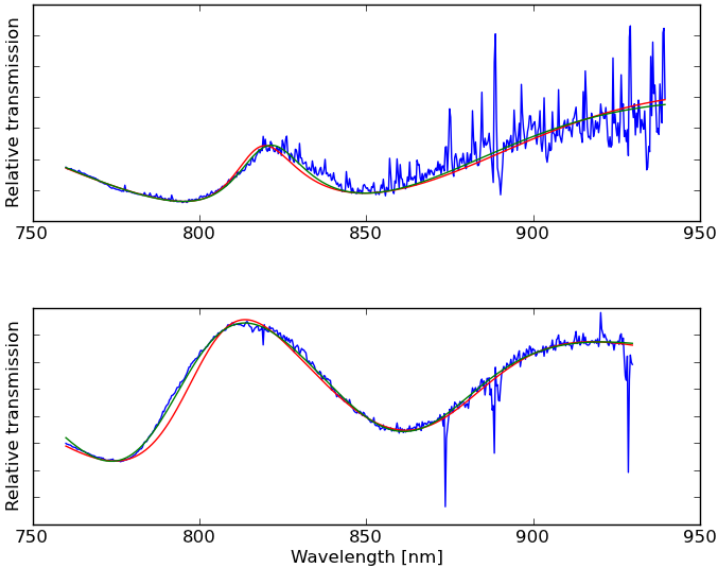

(a) Allowing an additional phase offset ϕ_{dt} in the fitting routine leads to good fitresults.

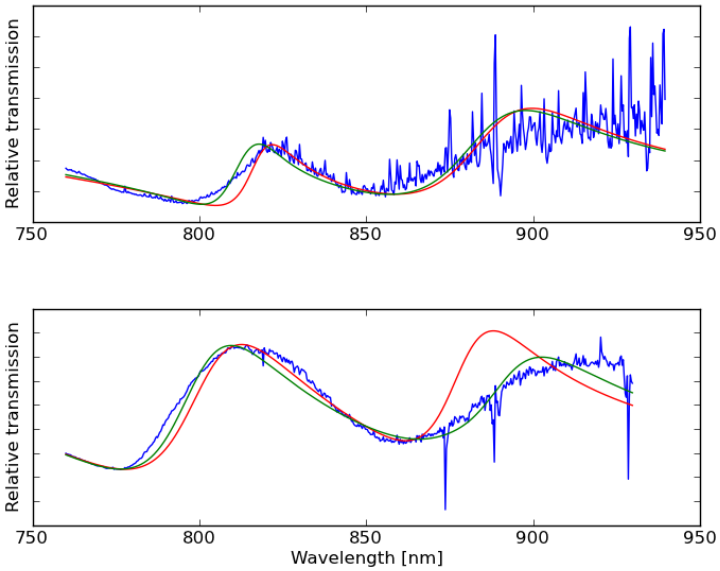

(b) Denying an additional phase offset ϕ_{dt} , by setting $\phi_{\mathrm{dt}} = 0$, leads to less optimal fitresults.

Figure 4.3.3: ODR fitting results to the transmission spectrum of the 338 nm (top) and the 486 nm (bottom) structure, with (a) and without (b) allowing an additional phase offset ϕ_{dt}.

the case of the first peak expected at 787 nm. The second peak, expected at 854 nm, did not show a clear moving trend, but it too is consistently redshifted by roughly 2% compared to the expected position. When looking at comparable results in literature there is a clear discrepancy between the results obtained here and those found in literature. Calculations done by SALOMON [14] showed a 'slight redshift' of the transmission maxima for *increasing* holesize while both calculations and measurements done by Li [9] showed a dependence of the position of both transmission peaks and transmission dips on the holesize that, too, led to a blueshift for smaller holes. As was shown by VAN DER MOLEN [10], a redshift can occur when, using rectangular holes, the aspect ratio of the open area of the holes is increased. To account for the observed redshift up to 4%, the aspect ratio would be required to be near 1.35, which is clearly not the case in the aperture arrays studied in this research.

Looking back at the results as were obtained in this research, one could try to explain the discrepancy by calculation errors in determining the position of the expected SPP resonances. Any calculation error in the position of the resonance, however, would still fail to account for the *trend* in the shifting of the resonance positions. Based on analysis of the functions used in determining the positions of the resonances any calculation error is expected to be of the order of a few nanometer while the observed discrepancy would require at least an error of approximately 20 nm.

Considering the experiment that was done in this research, and especially noting the holesizes that were used, an explanation might be found in this holesize. As in general research on EOT is done in the small hole regime, where the wavelength of the incident light is below the cutoff wavelength, this experiment is not directly comparable to reported results in literature. In the setup under consideration here, holesizes varied from 160 nm up to 590 nm. As the associated cutoff wavelength then ranges from 450 nm up to 1300 nm respectively, it is immediately seen that for EOT effects resulting from an incident wavelength of $\sim$800 nm, the apertures will go through cutoff when they are made smaller. It is not directly clear how this will influence the overall transmitted spectrum, and it might be interesting to research this aspect as a follow-up to this research project.

Chapter 5

Conclusion

The setup that was built in this project and described in this thesis allows for reproducibly measuring EOT using an incoherent, white light LED. The resulting spectra can be qualitatively understood by assuming SPP mediated transmission where, depending on the phase of the transmitted light and corresponding constructive or destructive interference, the transmitted light can lead to either an increase or a decrease in overall transmission. The wavelength at which interference of the direct transmission with the SPP mediated transmission occurs can be calculated, using the theory as described in Chapter 2. When the interference peaks are not too much overlapping, an ODR fitting scheme can be used to extract the peak positions from the measured spectra. The determined peak positions differed from the theoretically expected positions, ranging from roughly -1% for large holesizes to +5% for the smallest aperture sizes. The RAYLEIGH anomaly appeared where it was to be expected, at 770 nm, corresponding to the periodicity of the structures.

Chapter 6

Outlook

The research as presented in this thesis has had a small spin-off project at the Atom Optics and Ultrafast Dynamics (AOUD) group where the research was done, which will be described in Section (6.1). An additional project to further clarify the behaviour of apertures in gold layers is in preparation, and will be treated in the second section. The final section will give a short description of the research project on the trapping of Rubidium atoms that is being initialized within the AOUD group.

6.1 Infrared Tail of the LED

The first spin-off of the research project is directly related to the behaviour of the LED in this setup. The infrared emission tail that was observed, as can be seen in the inset in Figure (3.3.1b), was an unexpected yet welcome feature of the LED. The time dependence of the emission spectrum, as shown in Figure (3.3.2), however led to a constraint on the integration time for measurements. As a small research project bachelor students from the University College Utrecht (UCU) have measured a LED of the same type as was used in this research. They have determined the temperature dependence of the emission spectrum and concluded that the power falloff is due to heating of the LED, resulting from the 0.9 A of current that it draws during operation. Additionally the results show that the total current through the LED also influences the relative amount of infrared light that is being emitted. It is known from the specifications that the emission spectrum changes in the 480–780 nm range, but how this would affect the infrared tail was yet unknown. Additionally, the LED the UCU students have measured appeared to have the infrared tail start at roughly 900 nm instead of near 1000 nm, which makes it interesting to measure a set of these LED's in the future, possibly replacing the current LED by one that has a significant broader and more intense emission above 850 nm.

6.2 Hole Versus Periodicity

A future project will focus on determining the influence of the periodicity of the hole array (the EOT) versus the single hole. Although based on aperture theory a single hole is expected to show only the wavelength dependence on incident light as predicted by BETHE ($\sim \lambda^{-4}$), it would be worth measuring the transmission through a single hole to compare the measured transmission to the spectra as was determined in this project. This will require a sample on which both hole arrays and single holes of the same size are present. If such a measurement is done it might become possible to clarify some features that are present in this spectrum but are not predicted by SPP resonances. Note, for example, both the rise of the plateau at 690–760 nm, where one would expect a λ^{-4} falloff, and the emergence of the unexpected peak near 1000 nm in Figure (4.2.1).

Additionally, if the holes are made to span the same range of holesizes as were researched in this project, the effect of going through the cutoff wavelength by changing holesizes can be studied, which might in turn shed light on the red shifting of the SPP resonances as was reported in this research.

6.3 Rubidium Atoms Near Surfaces

As was stated in the Introduction, Section (1.2), one of the motives for this research on EOT through periodic arrays in a gold film was based on the starting of a new research project within the AOUD group. This project aims at researching interactions of Rubidium atoms with metal surfaces when these atoms are trapped and kept near the surface but prevented from making contact. The trapping of the atoms will be done using standing wave patterns from interfering and counterpropagating laser beams. Counterpropagation of the laser beam near the surface is achieved by using the reflection of the incident laser off the surface. By using a reflective surface with a periodic hole structure in it, the wavefront of the back reflected laser beam can be modified to lead to complex interference patterns which in turn can be used to create specific trap configurations. As in this case SPP resonances are expected to occur in a similar way as were researched in this thesis, using a periodic hole structure for reflection will allow studying the interaction of Rubidium atoms with the evanescent field of the SPP's by determining the change in the EOT spectrum resulting from SPP's coupling to Rubidium.

Bibliography

[1] H.A. Bethe, *Theory of Diffraction by Small Holes*, Physical Review 66 (1944) 163-182

[2] P.T. Boggs, R.H. Byrd, J.R. Donaldson and R.B. Schnabel, *ODRPACK: Software for weighted Orthogonal Distance Regression*, http://www.scipy.org/doc/api_docs/SciPy.odr.html

[3] Q. Cao and P. Lalanne, *Negative role of Surface Plasmons in the transmission of metallic gratings with very narrow slits*, Physical Review Letters 88 (2002) 057403

[4] T.W. Ebbesen, H.J. Lezec, H.F. Ghaemi, T. Thio and P.A. Wolff, *Extraordinary Optical Transmission through sub-wavelength hole arrays*, Nature 391 (1998) 667-669

[5] H. Gao, J.M. McMahon, M.H. Lee, J. Henzie, S.K. Gray, G.C. Schatz and T.W. Odom, *Rayleigh Anomaly-Surface Plasmon Polariton resonances in palladium and gold subwavelength hole arrays*, Optics Express 17 (2009) 2334-2340

[6] R. Gordon, D. Sinton, K.L. Kavanagh and A.G. Brolo, *A new generation of sensors based on Extraordinary Optical Transmission*, Accounts of Chemical Research 41 (2008) 1049-1057

[7] J.D. Jackson, *Classical Electrodynamics*, Second edition, Wiley (1975)

[8] C. Kittel, *Introduction to Solid State Physics*, Seventh edition, Wiley (1996)

[9] JY. Li, YL. Hua, JX. Fu and ZY. Lia, *Influence of hole geometry and lattice constant on Extraordinary Optical Transmission through subwavelength hole arrays in metal films*, Journal of Applied Physics 107 (2010) 073101

[10] K.L. van der Molen, K.J. Klein Koerkamp, S. Enoch, F.B. Segerink, N.F. van Hulst and L. Kuipers, *Role of shape and localized resonances in Extraordinary Transmission through periodic arrays of subwavelength holes: Experiment and theory*, Physical Review B 72 (2005) 045421

[11] E.D. Palik et al, *Handbook of Optical Constants of Solids, Volume 1*, First edition, Academic Press (1985)

[12] J. Prangsma, *Local and dynamic properties of light interacting with subwavelength holes*, PhD Thesis (2009)

[13] Lord Rayleigh, *On the Dynamical Theory of Gratings*, Proceedings of the Royal Society A79 (1907) 399-416

[14] L. Salomon, F. Grillot, A.V. Zayats and F. de Fornel, *Near-Field Distribution of Optical Transmission of Periodic Subwavelength Holes in a Metal Film*, Physical Review Letters 86 (2001) 1110-1113

[15] T. Thio, H.F. Ghaemi, H.J. Lezec, P.A. Wolff and T.W Ebbesen, *Surface-Plasmon-Enhanced transmission through hole arrays in Cr films*, Optical Society of America B 16.10 (1999) 0740-3224/99/101743-06

[16] J. Weiner, *The Physics of light transmission through subwavelength apertures and aperture arrays*, Reports on Progress in Physics 72 (2009) 064401

[17] A.V. Zayats, I.I. Smolyaninov and A.A. Maradudin, *Nano-optics of Surface Plasmon Polaritons*, Physics Reports 408 (2005) 131-314

Acknowledgement

Big thanks to the following people:

Ole Mußmann for supervising my research project and for the hints and tips on the more practical side of the experiment. It made life quite a bit easier and the *stitch.py* script saved loads of time by seamlessly combining all the measured spectra.

Dries van Oosten for supervising my research and explaining to me, or hinting where I could find, everything I needed to know to do this research, and always standing ready with additional advise on solving problems I didn't even know I had.

Peter van der Straten for the conversations we had. The sheer knowledge and perspective you have on physics helped keeping me on my toes and forced me to realize time and again that nothing ever is what I expect it to be.

Pepijn Marcus for having re-done the measurements I did earlier, it showed not only the setup gave an unexpectedly good reproducibility, but the (time consuming) measurements in the IR region resulted in spectra of a better quality than I had.

Kira Klop for your patience and support and for keeping me motivated every time things got frustrating.

And last but not least:
Thank you, AOUD group, for allowing me to do this research and letting me do my experiment with the freedom I had, yet always being there to solve either technical or theoretical problem whenever I bumped into one. Doing a Master's research is about more than just turning the dials and interpreting the results as in the end there is always a team involved behind the scenes and the accompanying aspects of being a member of a group should never be underestimated. I really enjoyed being part of the group and learned a lot from it besides 'how to do physics'.